EMP monazite dating of granitoid deformation: implications for Neoproterozoic ductile shear zone tectonics to the west of the Delhi Fold Belt

Jana Just[a,*], Bernhard Schulz[b], Helga de Wall[a], Fred Jourdan[d] and Manoj K. Pandit[c]

[a] Geozentrum Nordbayern, Schlossgarten 5, D-91054 Erlangen, Germany

[b] Institut fuer Mineralogie der TU Bergakademie, Freiberg/Saxony, Germany

[c] Department of Geology, University of Rajasthan, Jaipur -302004 India

[d] Western Australian Argon Isotope Facility, Department of Applied Geology and JdL-CMS, Curtin University of Technology, G.P.O. Box U1987, Perth, Western Australia 6845, Australia

*Corresponding author. Fax: +49-09131-852-9295, e-mail address: jana.just@geol.uni-erlangen.de

Abstract

Geochronology using the in-situ "chemical" Th-U-Pb dating of monazite with the electron microprobe is used to unravel the Neoproterozoic tectonothermal history of the “Erinpura” granitoid terrane in the foreland of the Delhi Fold Belt in the NW Indian craton. These granitoids were partially deformed during shearing activity. Monazites from the Erinpura Granite recorded two main events: (1) A 863 ± 23 Ma event which is considered as a granitoid protolith crystallization age and (2) a 775 Ma event, interpreted as recrystallization as well as newly formed Th-poor monazites, related to a shearing overprint. Some components of the Erinpura granitoid suite, such as the Siyawa Granite and granite near

Sirohi town show evidence of migmatization. This migmatization event is documented by anatexis and monazite crystallization at 779 ± 16 Ma. The data indicate that the anatectic event marks the beginning of ductile shear zone deformation, which lasted until 736 ± 6 Ma. This age mark is also constrained by the Ar-Ar muscovite age data obtained from shear zone rocks in the Sirohi Belt.

Keywords: Erinpura Granite, NW India, EMPA monazite dating, Ar-Ar muscovite age, shear zone

1. Introduction

Geological relationships and structural fabric analyses can reveal the information on relative chronology of events; however, absolute age constraints are required in evaluating crustal deformation and continental tectonics and paleogeographic reconstructions. A number of age dating methods are now available with reliable accuracy levels. Choice of the dating method is largely governed by the objective of the age dating exercise (whether emplacement age, metamorphic age, provenance age or age of the last thermal event) and mineralogical characteristics of rocks. Furthermore, obtaining the age constraints on complexly deformed Precambrian rocks is difficult because of the limitation of the conventional whole rock dating methods in resolving the ages of various deformation events. In such cases a combination of microstructural data and in-situ geochronological analysis of fabric-defining major or accessory mineral phases in thin sections can be performed. In such cases the in-situ mineral-chemical analysis with electron-microprobe Th-U-Pb dating of monazites (EMP-CHIME method) can be

considered as an appropriate method. Monazite can crystallize in a rock in response to the successive tectono-thermal events (e.g., Forster et al., 2002, 2004; McFarlane et al., 2006; Mahan et al., 2006; Tchato et al., 2009). Therefore its analysis can be used for geochronometry of crystallization ages through a long and polyphase history of geological events like metamorphism, migmatization and shear zone formation (Suzuki and Kato, 2008; Kusiak, et al. 2008). The monazite grains thus can be used to date the corresponding geological event. Notwithstanding the relatively higher levels of uncertainty as compared to some other geochronological methods (e.g., U – Pb zircon) the particular advantages of the Th-U-Pb dating method of monazite is its potential to record several successive thermal events in microstructural controlled in-situ dating. We have applied the in-situ EPMA – CHIME monazite dating method to evaluate the tectono-thermal history of the Neoproterozoic Erinpura Granite terrane in NW India (Fig. 1a) which shows evidence of a protracted tectonothermal history. The NW Indian terrane which was successively deformed during the Neoproterozoic also occupies a key position in the paleogeographic reconstruction of Late Precambrian Rodinia accretion, break-up and the subsequent dispersal (Dalziel, 1991). In most paleogeographic reconstruction models (Torsvik et al., 2001; Meert, 2003, Li et al., 2008), the NW Indian block is shown to represent the western margin of the supercontinent Rodinia. Deciphering its evolutionary history requires a proper understanding of magmatic, metamorphic and deformation events.

We have recently carried out monazite EPMA studies on the Neoproterozoic granitoids around Sirohi town in NW India which forms part of the granitoid terrane from along the western margin and foreland of Meso-Neoproterozoic Delhi Fold Belt (DFB). These granitoids have been loosely described as 'Erinpura Granite' which includes a variety of variably deformed granitoids that occur in a vast terrain in the western foreland of the DFB. They have been conventionally described as the manifestations of late thermal events relative to the 1 Ga Delhi Orogeny (Gupta et al., 1980). Available age data on Erinpura Granite are scarce. For a considerable time the whole rock Rb – Sr age data of 820 Ma for Pali area and 830 Ma for type Erinpura (Choudhary et al., 1984) remained the major geochronologic work on Erinpura Granites. In the recent years more precise U – Pb ages (836+7/-5 Ma for Siyawa granite by Deb et al., 2001; 800 Ma for Pali granite by van Lente et al. (2009) have been published. van Lente et al. (2009) have also reported a discordant age of 873 Ma for a small tonalite body from Pali area. The 'Erinpura Granite' terrane shows localized zones of high-strain and regions of migmatitic to anatectic character, the latter so far regarded as textural variations within the late syn-collisional granite gneisses (Roy and Sharma, 1999). Mutual relationships and evolution of the shear zone formation and migmatization have not been understood properly.

This paper presents the results of a microstructural controlled monazite EPMA dating of different components of Erinpura Granite around Sirohi town in NW India (Fig. 1b). The results are discussed and interpreted to offer constraints on the timing of tectono-thermal events for the 900 - 700 Ma time window. This period is significant in the context of break-up history of the

supercontinent Rodinia wherein the NW Indian block along with the neighbouring northern Madagascar and the Seychelles lay along its western margin (Torsvik et al., 2001).

2. Geological setting

The Precambrian geology of NW India includes an Archean basement (3.3 to 2.5 Ga) and overlying Proterozoic Aravalli and Delhi Fold Belts (Fig. 1a). The latter fold belt can be discriminated into an older nothern section (North Delhi Fold Belt) with Andean-type magmatism of 1.8 Ga (Kaur et al., 2009) and a younger southern section (South Delhi Fold Belt) with an Grenvillian age (~1 Ga) arc setting (Pandit et al. 2003) resulting from east directed subduction beneath the Archean-Paleoproterozoic craton (Khan et al., 2005; Roy and Jakhar, 2002). This subduction can be related to the global scale tectonics resulting in amalgamation of crustal blocks to form the Supercontinent Rodinia. Evidence of Grenvillian age thermal events along the western flank of the Delhi Fold Belt (DFB) are seen in the form of 987 Ma (± 6.4) rhyolites of the so called Sendra-Ambaji-Ajmer sector (Deb et al., 2001) and 968.3 Ma (± 1.2) calc-alkaline Sendra granitoids (Pandit et al., 2003). The rocks of DFB are metamorphosed up to amphibolite facies and repetitively deformed and subsequently intruded by supposedly late collisional granitoids (Erinpura Granite – Heron, 1953). This magmatic event has resulted in 860 – 830 Ma granite intrusions (Choudhary et al., 1984; Deb et al., 2001; van Lente et al., 2009), seen all over in the southern segment of the DFB as well as in the foreland. These intrusions consist of apparently undeformed to

variable deformed granites and granite gneisses. These granitoids form the basement for the metasediments of Sirohi Group. The Erinpura Granite and Sirohi Group have been involved in a common deformation episode and are overlain by the felsic volcanics and intruded by granites of the 770 – 750 Ma Malani Igneous Suite.

The region around Sirohi town in SW Rajasthan (Fig. 1b) shows exposures of Erinpura Granites and shear zones. A prominent shear zone (up to 100 m wide, approx. 1.5 km east of Sirohi) defines a tectonic contact between Erinpura Granite and sediments of Sirohi Group. There are evidence of migmatization and anatexis along the shear zone. For the present study the Erinpura Granite, shear zone rocks as well as migmatised members of the granite were sampled. In addition, the Siyawa Granite (Fig. 1b) was also sampled, which represents Erinpura Granite emplaced within the DFB. The sampling sites for the present study are described as follows:

2.1. Shear zone in Erinpura Granite (SRS)

A prominent shear zone is exposed in a road section ca. 1.5 km SE of Sirohi town and is called SRS (Sirohi Road Section). This site (24° 52.503`N, 72° 52.871`E, site 1 in Fig. 1b) is a high-strain zone where Erinpura granite gneiss documents progressive development (Fig. 2a-c) of protomylonite, mylonite to ultramylonite fabric under the effect of shearing. Structural fabrics revealed steeply SE and partially NW dipping foliations and down-dip lineations. The adjacent metasediments of the Sirohi Group (meta-carbonates and mica schists) show a tectonic contact and the same structural fabric as the

mylonites, indicating a common deformation history. For monazite dating of the shear zone one sample from the megascopically least strained part (protolith) and another two samples from within the shear zone (mylonite and ultramylonite) were collected (site 1 in Fig. 1b). For muscovite $^{40}Ar/^{39}Ar$ dating we selected one sample from an equivalent mylonite in the SRS, ca. 1 km far away from the sample location for monazite dating.

2.2. Anatectic derivative of Erinpura Granite

Near the village Veerwara (24° 50.101`N, 72° 59.027`E, site 2 in Fig. 1b) the Erinpura Granite shows various features of migmatization (Fig. 2d, e) ranging from felsic melt veining to formation of melt pockets, still controlled by the prevalent foliation, to cross-cutting veins of felsic melt and areas of diatexite to remobilization into anatectic melts. This melt has been mobilized and crystallized into outcrop scale granitic bodies. This anatectic part of the Erinpura Granite is a medium-grained, two mica granite and has been sampled for monazite dating. It has a faint NW trending steep foliation and down-dip lineation.

3.3. Siyawa Granite

The Siyawa Granite (24° 25.834`N, 72° 46.281`E, site 3 in Fig. 1b) is a medium-grained, two mica granite gneiss with well-developed garnet crystals within feldspar-rich segregates (Fig. 2f). It intrudes the metasedimentary rocks of the DFB in the southern part of the Ambaji-Sendra sector. Deb et al. (2001) dated intrusion of the Siyawa Granite at 836 +7/-5 Ma (U – Pb age of

zircon) and 826 ± 5 Ma (U – Pb age of monazite), the latter data either represents slow cooling or a younger thermal event.

3. Analytical methods

After petrographic inspection polished thin sections of the samples described above were inspected by backscattered electron imaging (BSE) for monazite (LREE, Th) PO_4 occurrence, their microstructural positions and reaction structures. The subsequent in-situ "chemical" Th-U-Pb dating of monazite by electron microprobe analysis (EMP monazite dating, Suzuki et al., 1994 Montel et al., 1996; Dahl et al., 2005a, 2005b; Williams et al., 2006) is based on the observation that the concentration of common lead is negligible when compared to radiogenic lead resulting from decay of Th and U (Parrish, 1990; Cocherie et al., 1998), and on the premise that no radiogenic lead loss has occurred since the closure of the system. Diffusion experiments by Cherniak et al. (2004) showed that monazite is the most Pb-retentive accessory mineral. As Th concentrations are 3 - 14 wt%, radiogenic lead can be analyzed by EMP in Palaeozoic and older monazite. Analysis of Th, U and Pb for calculation of monazite model ages, as well as for Ca, Si, LREE and Y for corrections and evaluation of the mineral chemistry were carried out on a JEOL JXA 8200 (Geozentrum Nordbayern, University of Erlangen-Nürnberg) at 20 kV, 100 nA, and a beam size of 5 µm (*for details please see* Schulz et al., 2007).

Mα1 lines of Th and Pb and the Mβ1 lines for U of a PETH crystal were selected for analysis. Resulting errors (1σ) are typically 1.0 %, 0.20 % and 1.30 % for Pb, Th and U, respectively, based on counting statistics. The lines Lα1 for La, Y, Ce; Lβ1 for Pr, Sm, Nd, Gd and Kα1 for P, Si and Ca were chosen. Orthophosphates of the Smithsonian Institution were used as standards for REE analysis (Jarosewich and Boatner, 1991; Donovan et al., 2003). Calibration of PbO was carried out on a vanadinite standard, while U was calibrated on an appropriate glass standard with 5 wt% UO_2. The Madmon monazite (Schulz et al., 2007), dated by SHRIMP at 496 ± 9 Ma and numerous Pb-Pb-TIMS monazite evaporation data (K. Bombach, Freiberg, unpublished analytical method) at 497 ± 2 Ma, contains ThO_2 at around 10 wt%. The ThO_2 in Madmon was previously determined by LA-ICPMS and by the microprobe at University of Salzburg (Finger and Helmy, 1998) and was used for calibration of ThO_2 as well as for the control of data. Interference of YLγ on the PbMα line was corrected by linear extrapolation after measuring several Pb-free yttrium glass standards as proposed by Montel et al. (1996). An interference of ThMγ on UMβ was also corrected by using a Th-glass standard. Interference of a Gd-line on UMβ needs correction when Gd_2O_3 in monazite is > 5 wt %. These parameters matched the analytical problems discussed in Jercinovic and Williams (2005) and Jercinovic et al. (2008) in the best way (Schulz et al., 2007). For each single analysis, a chemical age (CHIME) and a 2σ error based on the Pb counting statistics was calculated. When the regression of several single data points in the ThO2* vs. PbO diagram (Suzuki et al., 1994) defines an isochron forced through zero (Montel et al., 1996), a weighted mean age involving a 2sigma error was calculated

(Ludwig, 2001) from this population. These weighted mean ages are reported in the text and figures and coincide with the ages given by the slopes of the isochrons. Other possible sources of error, such as standardization, matrix effect correction, YLγ-on-PbMα correction and instrumental drift were not taken into account. Therefore the given error on the calculated ages should be considered as a minimum error. The dating routine has been successfully applied for dating granitoids (Djouka-Fonkwe et al., 2007) and garnet metapelites (Schulz, 2009).

For the $^{40}Ar/^{39}Ar$ dating we selected one sample from the sheared metasediments of the Sirohi Group in the Erinpura share zone (site 1 in Fig. 1b) and separated unaltered, optically transparent, 500-1000 µm-size, muscovite. Muscovite grains were carefully hand-picked under a binocular microscope and rinsed with distilled water in an ultrasonic cleaner. Samples were loaded into a large well of one 1.9 cm diameter and 0.3 cm depth aluminum disc. This well was bracketed by small wells that included Fish Canyon sanidine (FCs) used as a neutron fluence monitor for which an age of 28.03 ± 0.08 Ma was adopted (Jourdan and Renne, 2007). The discs were Cd-shielded (to minimize undesirable nuclear interference reactions) and irradiated for 25 hours in the Hamilton McMaster University nuclear reactor (Canada) in position 5C. The mean J-values computed from standard grains within the small pits is 0.008843 ± 0.000019 (0.22%). Mass discrimination was monitored using an automated air pipette and provided a mean value of 1.00417 ± 0.0037 per dalton (atomic mass unit). The correction factors for

interfering isotopes were ($^{39}Ar/^{37}Ar$) Ca = 7.30x10-4 (± 11%), ($^{36}Ar/^{37}Ar$)Ca = 2.82x10-4 (± 1%) and ($^{40}Ar/^{39}Ar$)K = 6.76x10-4 (± 32%).

The $^{40}Ar/^{39}Ar$ analyses were performed at the Western Australian Argon Isotope Facility at Curtin University, operated by a consortium consisting of Curtin University and the University of Western Australia. A single-grain muscovite samples was step-heated using a 110 W Spectron Laser Systems, with a continuous Nd-YAG (IR; 1064 nm) laser rastered over the sample during 1mn to ensure an homogenously distributed temperature. The gas was purified in a stainless steel extraction line using three SAES AP10 getters and a liquid nitrogen condensation trap. Ar isotopes were measured in static mode using a MAP 215-50 mass spectrometer (resolution of ~600; sensitivity of 2x10-14 mol/V) with a Balzers SEV 217 electron multiplier mostly using 9 to 10 cycles of peak-hopping. The data acquisition was performed with the Argus program written by M.O. McWilliams and ran under a LabView environment. The raw data were processed using the ArArCALC software (Koppers, 2002) and the ages have been calculated using the decay constants recommended by Steiger and Jäger (1977). Blanks were monitored every 3 to 4 steps and typical ^{40}Ar blanks range from 1 x 10-16 to 2 x 10-16 mol. Our criteria for the determination of plateau are as follows: plateaus must include at least 70% of ^{39}Ar. The plateau should be distributed over a minimum of 3 consecutive steps agreeing at 95% confidence level and satisfying a probability of fit (P) of at least 0.05. Plateau ages are given at the 2σ level and are calculated using the mean of all the plateau steps, each weighted by the inverse variance of their individual analytical error. The uncertainties on the

$^{40}Ar^*/^{39}Ar$ ratios of the monitors are included in the calculation of the integrated and plateau age uncertainties, but not the errors on the age of the monitor and on the decay constant (internal errors only, see discussion in Min et al., 2000).

4. Results

4.1 Shear zones in Erinpura Granite (SRS)

The protolith of the shear zone rocks is a massive granite gneiss (Fig. 2a), which shows weakly developed foliation parallel to the trend of the shear zone (NE-SW). Mineral constituents include large zoned K-feldspar porphyroblasts (up to 10 cm in size) within a groundmass comprising biotite, plagioclase, muscovite, quartz. Accessory minerals include Fe-Ti oxides, epidote, chlorite, zircon, apatite, tourmaline and monazite. Petrographic examination of feldspars revealed microstructures related to both brittle and ductile deformation. Brittle fracturing of K-feldspar, patchy undulose extinction and deformation twins in albite indicate deformation under low grade conditions, i.e. below 400 °C. Transition from brittle to ductile deformation is indicated by filling of microcracks with newly crystallized quartz, fine-grained recrystallized feldspar and mica (Fig. 3a). The ductile behaviour is also indicated by initially developed core-and-mantle structures, microkinking and sporadically myrmekitic and abundant flame-perthite. Myrmekitic intergrowths along the margins of K-feldspar porphyroblasts indicate a deformation-induced replacement of K-feldspar by plagioclase and

quartz (Simpson and Wintsch, 1989), probably at decreasing temperature or under retrograde metamorphic conditions (e.g., Shelley, 1993). Abundant microperthite with flame-shaped lamellae and strain-induced myrmekite indicate deformation under greenschist facies conditions at high differential stresses (Passchier and Trouw, 2005). In proximity to the shear zone mylonitic fabric with increasing degree of alignment of the ground mass components into the foliation, dominant core-and-mantle structures and progressive grains size reduction reveals the influence of high-strain shearing under medium (400 – 600 °C) grade conditions (Fig. 3b, c).

Two morphological types of monazite grains were observed in the Erinpura granitoids, the protolith and the mylonite. The first grain type occurs as large (>100 µm) rounded inclusions within feldspar grains and shows irregular and complex zoning patterns in BSE image, induced by variable Th-contents (Fig. 4a). In the ThO_2* vs. PbO diagram (Fig. 5a) such monazites show generally high Th content with ThO_2* > 6%. Among these large monazite grains, two age population domains were observed. The older age population defines an isochron and yielded a weighted mean age of 863 ± 23 Ma (MSWD = 0.043, P = 1.00). These grains or parts of them are considered as magmatic in origin, meaning the crystallization of magmatic monazite. The other group of younger age population in the same monazite grains forms isochron that is not so well-defined and the weighted mean age centers around 776 ± 29 Ma (MSWD = 0.37, P = 0.994). Such grains with two age populations are considered as magmatic in origin and overprinted by a later thermal event as indicated by the two isochrons. The chemical composition (Fig. 6a) shows

high Th content (ThO_2* > 6 wt%) and a wide variation in Y_2O_3, the latter rangeing from 0.2 to 3.2 wt%. The Si content in magmatic monazite reveals a tendency toward an increase from old to younger grain domains indicating a thermal overprint. This is also seen in the Ca (CaO) content, however, only gently indicated.

The second morphological type of monazite is associated with magmatic biotite and occurs as irregular, small grains (20 and 50 µm) within the mika flakes (Fig. 4b). In the ThO_2* vs. PbO diagram such grains are generally poor in Th content (ThO_2* < 3.5 wt%) and plot only along a single isochron. These small grains are referred to as recrystallized new monazite. They are uniformly rich in Y, ranging between 1.05 and 2.6 wt%, but poor in Ca and Si (Fig. 6a). The EMP-CHIME Th-U-Pb data revealed an age of 775 ± 57 Ma (MSWD = 0.054, P = 1.00). This age is afflicted by a considerable error due to rather low Pb contents as a consequence of low Th contents. These newly formed grains revealed similar ages with a younger age population in the large magmatic monazite grains. Therefore, we calculated cumulative data points of the newly formed grains and the younger areas in magmatic grains resulting an age of 775 ± 26 Ma (MSDW = 0.19, P = 1.00) that can be related to a younger overprint of the Erinpura Granite, probably a thermal event.

For comparison single grain muscovite sample RT-01 (N 24° 52.207, E 72° 53.112, site 1 in Fig. 1a) from similar sheared granite in the SRS shear zone yielded a well-defined plateau age at 736 ± 6 Ma (MSWD = 0.62, P = 0.76)

including 87% of ^{39}Ar released (Fig. 7). No statistically meaningful inverse isochrone age could be calculated due to a strong clustering of the data near the $^{39}Ar/^{40}Ar$ axis.

4.2 Anatectic derivates of Erinpura Granite

Petrographic observations affirm a weak planar anisotropy with σ-clasts and recrystallization of feldspar in the anatectic granite (Fig. 3d). Larger feldspar clasts show microcracks partially filled with recrystallized feldspar, biotite, quartz and mica that provide evidence of ongoing deformation during cooling. Large magmatic quartz grains show grain boundary bulging and recrystallization at the margins. Abundant myrmekite, especially grown along bands of weakness in K-feldspar (Fig. 3e), affirm that stress was active during cooling. These microstructural features indicate medium-grade deformation conditions subsequent to migmatic crystallization.

Unaltered monazite grains (Fig. 4d) occur as inclusions in feldspar or quartz and have grain sizes <50 μm. When associated with biotite they are partially decomposed and surrounded by coronas of apatite, Th-silicates and epidote (Fig. 4e). In the ThO_2* vs. PbO diagram (Fig. 5b) all measured domains plot along the 779 Ma isochron indicating single generation. The chemical composition (Fig. 6a) is quite distinct with relatively high Th (ThO_2* > 10 %) and Si (SiO_2 > 1 %) contents. The Y and Ca define a wide compositional range, similar to the overprinted monazites present in mylonites from the shear zone. The EMP-CHIME Th-U-Pb data revealed an age of 779 ± 16 Ma

(MSWD = 0.26; P = 1.00) that is interpreted as crystallization age of newly formed granite from anatectic melts.

4.3 Siyawa Granite

Petrographic evidence of strong alteration is seen as intense sericitization of feldspars and chloritization of biotites. Old feldspar grains show irregular boundaries due to decomposition, accompanied by sericitization, myrmekite and subgrain formation (Fig. 3f), probably caused by a later deformation under medium-grade conditions. Undulose extinction, rare feldspar recrystallization and the absence of core-and-mantle structures support the assumption that deformation took place under low-grade conditions (< 400° C).

The EMPA-CHIME data reveal a wide range of ages and in the ThO_2* vs. PbO diagram (Fig. 5c) these data define three isochrons (~835, ~782 and ~736 Ma), which imply several stages of thermal overprint in monazite. The oldest two grains on the 835 Ma isochron are very small (< 20 μm) and occur as isolated grains within quartz or feldspar (Fig. 4f). These are interpreted as magmatic monazites that were overprinted by later thermal events with a strong activities at 782 Ma and 736 Ma (the corresponding EMPA-CHIME data account 782 ± 14 Ma (MSWD = 0.29; P = 0.998) and 736 ± 14 Ma (MSWD = 0.13; P = 1.00)). All the small monazite grains are porous and show irregular and complex zoning patterns in BSE image, induced by variable Th-contents. Bright areas (higher Th-contents) represent relatively

older domains and darker areas (lower Th-contents) correspond to relatively younger domains (Fig. 4g). However, all monazites in the Siyawa Granite in general show high Th- (> 14% ThO_2*), high Ca- (> 2% CaO) but variable Y- and Si-contents (Fig. 6b).

5. Discussion and interpretation

The Erinpura Granite is a composite granitoid terrane with evidence of migmatization, anatexis and shearing. Although Sharma (1996) and Roy and Sharma (1999) reported these features they have not been understood properly in terms of the process and timing.

We have obtained the oldest age of 863 ± 23 Ma for the Erinpura Granite (site 1 in Fig. 1a). Two monazite grains in Siyawa Granite lie along the 835 Ma isochron, which we interpret as the protolith age. These data are within the reported time span on the Erinpura terrane (860 to 830 Ma) that also include the whole rock Rb – Sr ages of 830 and 820 Ma, reported by Choudhary et al. (1984). As the region shows evidence of thermal reworking, the validity of whole rock Rb – Sr ages to represent the crystallization ages is doubtful. The U – Pb zircon age of 836 +7/-5 Ma (Deb et al., 2001) gives a precise age for the emplacement of Siyawa Granite, but as it has a different tectono-thermal history than the type Erinpura Granite on account of obvious difference in the fabric and mineral composition (Fig. 2a, f) more reliable U – Pb zircon ages from the type Erinpura terrane are required.

The reported ages prior to the present study also imply that entire Erinpura terrane is a product to a single thermal event. The microstructure controlled monazite dating (present study) gives a distinct younger age for the formation of shear zones indicated in the age of (hydro-) thermally overprinted (776 ± 29 Ma) monazites as well as the newly formed (775 ± 57 Ma) ones. These two generations of monazite can be discriminated by variation in their chemical composition. While the magmatic monazite shows relatively high Th-contents (> 6% ThO_2*) and a wide range of Y-content (0.2 to 3.2 wt %), the newly formed monazite has generally low Th-content (< 3.5% ThO_2*) and relatively higher Y-content (> 1.05% Y_2O_3). Medium grade conditions around 400 – 600 °C, as seen in microstructural fabric of host minerals such as feldspars, and elevated differential stresses during deformation, probably triggered partial mobilization of magmatic monazite and crystallization of new monazite at distinct microstructural sites (Seydoux-Guillame et al., 2002, Mahan et al., 2006). This interpretation is further substantiated by the low Th-contents of the newly formed grains (Fig. 6a, triangles) indicative of a hydrothermal origin of monazite (e.g., Schandl and Gorton, 2004; Kempe et al., 2008). However, progressive deformation of the granite gneiss led to decomposition of monazite and finally to a complete disappearance in the ultramylonites.

In the anatectic terrane a syn-kinematic nature of melt generation and melt migration is evident from field relationships and microstructural findings. The monazite dating has yielded crystallization age of mobilized anatectic melt of 779 ± 16 Ma. There is no indication for an older monazite generation as seen

in the SRS shear zone and in the Siyawa Granite (please see histograms in Fig. 5). It can be clearly stated that the anatectic event is not related to the "Erinpura history" of the Delhi orogeny.

The timing of anatexis is more or less coeval with the shearing in Sirohi section (SRS). On the basis of the data sets it is possible to present a geochronological history of events. However, the field observations suggest that the shearing started prior to anatexis, as seen by blocks of sheared Erinpura gneiss, picked up and transported by the melt. This thermal event is also picked up in the Siyawa Granite where a dominant 782 ± 14 Ma overprint is seen in the magmatic monazites (Fig. 4g). This is also the most prominent age group in the Siyawa Granite suggesting a large regional extension. Feldspar-rich schlieren with large garnet crystals (up to 2 cm) were possibly formed during this thermal event and indicate relatively high temperatures because schlieren are common within granite-associated migmatites.

The $^{40}Ar/^{39}Ar$ cooling age at 736 ± 6 Ma (Fig. 7) for muscovite from the Sirohi section (SRS) provides an age constraint on the closure age below 350 ± 50 °C of this strong tectono-thermal event along the western boundary of the DFB. An additional age frequency maximum around 740 Ma in the monazite data of the Siyawa Granite (Fig. 5), which is also implied in the samples from the Sirohi area at ~750 Ma might also represent the cooling and marks the end of a protracted thermal history.

6. Implications on regional tectonics

The microstructure controlled monazite age data clearly establish two magmatic events; 863 ± 23 Ma and a younger tectono-thermal overprint ~780 – 736 Ma resulting in shearing and anatexis of the Erinpura granites.

The older age represents the emplacement age while the younger age can be related to tectono-thermal event that falls into the time interval known for the Malani magmatism with U – Pb ages of zircon at 770 – 750 Ma for Malani Igneous Suite (MIS) rhyolites and granites (Torsvik et al., 2001; Gregory et al., 2009; van Lente et al., 2009). van Lente et al. (2009) have dated rhyolite flows SE of Sirohi town (so-called Sindreth rhyolites), which yielded precise ages of 767 ± 3 Ma. These rhyolites overlay the deformed (folded, sheared) Erinpura/Sirohi sequence and therefore this age provides a lower age limit for the shear zone activity which is in good agreement with our data.

It can be concluded that the tectono-thermal episode, which is now recognized along the western margin of the DFB, is related to the Malani magmatism and not a late event of the Delhi orogeny as stated in earlier studies (Gupta et al., 1980). The field relationships point to an early event in the history of the Malani Igneous Suite (MIS). Cooling and thus termination of the thermal event can be inferred from the well-defined muscovite $^{40}Ar/^{39}Ar$ plateau age at 736 ± 6 Ma. The sequence of dated events by this study is compiled in Figure 8. Our study has clearly shown the synkinematic nature of new monazite formation during this thermal event. This also substantiates the findings of de Wall and Pandit (2007a) who ascribed the Mt. Abu batholith situated south of our study area as synkinematic intrusion that is a part of the MIS and unrelated to Delhi orogeny. A close geochemical

similarity also relates this deformed granitic complex to the MIS (Pandit and de Wall, 2010). Thus the NE trending oblong Mt. Abu might form a southern continuity of the anatectic terrane of Sirohi region with persistant NE tectonic trend (Fig. 9).

Syn-intrusional deformation fabrics in Mt. Abu granitoids (de Wall and Pandit, 2007b; de Wall et al., 2010; Pandit and de Wall, 2010) and evolution from sub-magmatic to solid-state fabrics in anatectic granites in Sirohi (this study) provide evidence that at least the early phase of the Malani thermal event in the proximity of the DFB was accompanied by tectonic stresses. This is further constrained by steep SE dipping foliations and pronounced down-dip lineations in the shear zones of the Sirohi area (Fig. 9), and in the Mt. Abu granites and orthogneisses. This fabric indicates that both areas are part of a single structural domain. A probable scenario is shown in Fig. 9. A NW-SE oriented maximum strain (σ_1) caused the formation of the NE-SW trending SRS shear zone and the associated fabrics in the Mt. Abu granites and gneisses. Hereby, the NE-SW trending DFB, by this time already a rigid body, acted as a back-stop during the deformation. Migmatites also evolved approximately at the same time and mark a continuation of the Mt. Abu granitoids.

Previous models have related Malani magmatic event to late Neoproterozoic crustal extension resulting from active rifting or plume activity (Bushan, 2000; Eby and Kochhar, 1990; Sharma, 2004; Li et al., 1999), whereby the

suggested tectonic frame was within a scenario of Rodinia break-up. The structural inventory as seen in this eastern part of the DFB foreland has been associated with the crustal convergence during the Delhi orogeny. These models need to be revised as our findings clearly link the structural imprint with the Malani thermal event.

Acknowledgements:

We are thankful to K.K. Sharma, M. Bestmann and H. Daxberger for support and company during field work and lively discussions. The microprobe analyses at GeoZentrum Nordbayern, Erlangen were assisted by N. Langhof.

References

Bhushan, S.K., 2000. Neoproterozoic magmatism of the Malani igneous suite western Rajasthan, India. Special Publication Series - Geological Survey of India, 55, 1, 318-331.

Cherniak, D.J., Watson, E.B., Grove, M. & Harrison, T.M., 2004. Pb diffusion in monazite: A combined RBS/SIMS study. - Geochim. Cosmochim. Acta 68, 829-840.

Choudhary, A.K., Gopalan, K. and Sastry, C.A., 1984. Present status of the geochronology of Precambrian rocks of Rajasthan. Tectonophysics, 105, 131 – 140.

Cocherie, A., Legendre, O., Peucat, J.J., Koumelan, A.N., 1998. Geochronology of polygenetic monazites constrained by in-situ microprobe Th-U-total lead determination: implications for lead behaviour in monazite. Geochimica et Cosmochimica Acta, 62, 2475-2497.

Dahl, P.S., Hamilton, M.A., Jercinovic, M.J., Terry, M.P., Williams, M.L. and Frei, R., 2005a. Comparative isotopic and chemical geochronometry of monazite, with implications for U-Th-Pb dating by electron microprobe: an example from metamorphic rocks of the eastern Wyoming Craton (U.S.A.). American Mineralogist, 90, 619–638.

Dahl, P.S., Terry, M.P., Jercinovic, M.J., Williams, M.L., Hamilton, M.A., Foland, K.A., Clement, S.M., Fiberg, L.M., 2005b. Electron probe (Ultrachron) microchronometry of metamorphic monazite: Unraveling the timing of polyphase thermotectonism in the easternmost Wyoming Craton (Black Hills, South Dakota). Am. Mineral. 90, 1712-1728.

Dalziel I.W.D., 1991. Pacific margins of Laurentia and East Antarctica as a conjugate rift pair: evidence and implications for an Eocambrian supercontinent. Geology, 19, 598-601.

Deb, M., Thorpe, R.I., Krstic, D., Corfu1, F. and Davis, D.W., 2001. Zircon U-Pb and galena Pb isotope evidence for an approximate 1.0 Ga terrane constituting the western margin of the Aravalli-Delhi orogenic belt, northwestern India. Precambrian Research, 108, 3-4, 195 – 213.

de Wall, H., Schöbel, S., Pandit, M.K., Sharma, K.K., Just, J., 2010. A record of ductile syn-intrusional fabrics to post solidification cataclasis: magnetic fabric analysis of Neoproterozoic Mirpur and Mt. Abu granitoids, NW India. J. Geol. Soc. India, Special Issue: Structural Geology – From Classical to Modern Concepts (January 2010, in press).

de Wall, H. and Pandit, M.K., 2007a. Preliminary magnetic susceptibility results on the Neoproterozoic Mt. Abu Granite, NW Indian craton; correlation between magnetic fabric and deformation. Geotectonic Res, 95, 87 – 99.

de Wall, H., and Pandit, M.K., 2007b. Cryptic fabrics in epiclastics of the Sindreth Group: evidence for Late Neoproterozoic deformation in the western foreland of the Delhi Fold Belt, Northwest India. Beringeria, 37, 33-40.

Djouka-Fonkwé, M.L., Schulz, B., Schüssler, U., Tchouankoué, J.-P, Nzolang, C., 2007. Geochemistry of the Bafoussam Pan-African I- and S-type granitoids in western Cameroon. Journal of African Earth Sciences, 50, 2-4, 148-167.

Donovan, J., Hanchar, J.M, Picolli, P.M, Schrier, M.D, Boatner, L.A, Jarosewich, E., 2003. A re-examination of the rare-earth-element *orthophosphate* standards in use for electron-microprobe analysis. The Canadian Mineralogist, 41, 1, 221-232.

Eby, G.N. and Kochhar, N., 1990. Geochemistry and petrogenesis of the Malani igneous suite, North Peninsular India. Journal of the Geological Society of India, 36, 2, pp.109-130

Finger, F and Helmy, H.M., 1998. Composition and total-Pb model ages of monazite from high-grade paragneisses in the Abu Swayel area, southern Eastern Desert, Egypt. Mineralogy and Petrology, 62, 3-4, 269-289.

Foster, G., Parrish, R.R., Horstwood, M.S.A., Cheney, S., Pyle, J., Gibson, H. D., 2004. The generation of prograde P-T-t points and paths; a textural, compositional, and chronological study of metamorphic monazite. Earth and Planetary Science Letters, 228, 125-142.

Foster, G., Gibson, H.D., Parrish, R.., Horstwood, M., Fraser, J. & Tindle, A. 2002. Textural, chemical and isotopic insights into the nature and behaviour of metamorphic monazite. Chem. Geol., 191, 183-207.

Gregory, L.C., Meert, J.G., Bingen, B., Pandit, M.K., Torsvik, T.H., 2009. Paleomagnetism and geochronology of the Malani Igneous Suite, northwest India: implications for the configuration of Rodinia and assembly of Gondwana. Precambrian Research, 170, 13 – 26.

Gupta, S.N., Arora, Y.K., Mathur, R.K., Iqbuluddin, Prasad, B., Sahai, T.N., Sharma, S.B., 1980. Lithostratigraphic map of Aravalli region, southern Rajasthan and northern Gujarat. Geol. Surv. India.

Heron, A.M., 1953. Geology of Central Rajputana. Memoirs of the Geological Survey of India, 79, 339p.

Jarosewich, E. and Boatner, L.A., 1991. Rare-earth element reference samples for electron microprobe analysis. Geostandards Newsletter, 15, 397-399.

Jercinovic, M.J., Williams, M.L., Lane, E.D., 2008. In-situ trace element analysis of monazite and other fine-grained accessory minerals by EPMA. Chem. Geol., 254, 3–4, 197–215.

Jercinovic, M.J and Williams, M.L., 2005. Analytical perils (and progress) in electron microprobe trace element analysis applied to geochronology: Background acquisition, interferences, and beam irradiation effects. American Mineralogist, 90, 526-546.

Jourdan, F. and Renne, P.R., 2007. Age calibration of the Fish Canyon sanidine $^{40}Ar/^{39}Ar$ dating standard using primary K-Ar standards. Geochimica et Cosmochimica Acta, 71, 387-402.

Kaur, P., Chaudhri, N., Raczek, I., Kroner, A. and Hofmann, A.W., 2009. Record of 1.82 Ga Andean-type continental arc magmatism in NE Rajasthan, India; insights from zircon and Sm/Nd ages, combined with Nd-Sr isotope geochemistry. Gondwana Research, 16, 1, 56-71.

Kempe, U., Lehmann, B., Wolf, D., Rodionov, N., Bombach, K., Schwengfelder, U., Dietrich, A., 2008. U/Pb SHRIMP geochronology of Th-poor, hydrothermal monazite; an example from the Llallagua tin porphyry deposit, Bolivia. Geochimica et Cosmochimica Acta, 72, 17, 4352-4366.

Khan, M.S., Smith, T.E., Raza, M., Huang, J., 2005. Geology, geochemistry and tectonic significance of mafic-ultramafic rocks of Mesoproterozoic Phulad ophiolite suite of south Delhi fold belt, NW Indian Shield. Gondwana Research, 8, 4, 553-566.

Koppers, A.A.P., 2002. ArArCALC-software for $^{40}Ar/^{39}Ar$ age calculations. Computers & Geosciences 28, 605–619.

Kusiak, M.A., Suzuki, K., Dunkley, D.J., Lekki, J., Bakun-Czubarow, N., Paszkowski, M., Budzyn, B., 2008. EPMA and PIXE dating of monazite in granulites from Stary Gieraltow, NE Bohemian Massif, Poland. Gondwana Research, 14, 4, 675-685.

Li, Z.X., Bogdanova, S.V., Collins, A.S., Davidson, A., de Waele, B., Ernst, R.E., Fitzsimons, I.C.W., Fuck, R.A., Gladkochub, D.B., Jacobs, J., Karlstrom, K.E., Lu, S., Natapov, L.M.,

Pease, V., Pisarevsky, S.A., Thrane, K., Venikovsky, V., 2008. Assembly, configuration and break-up history of Rodinia: A synthesis. Precambrian Research 160, 179 – 210.

Li, Z.X., Li, X.H., Kinny, P.D., Wang, J., 1999. The breakup of Rodinia: did it start with a mantle plume beneath South China? Earth and Planetary Science Letters, 173, 171-181.

Ludwig, K.R., 2001. Users manual for Isoplot/Ex rev. 2.49. 2. A geochronological toolkit for Microsoft Excel, vol. 1a. Berkeley Geochronology Center Special Publication, 55 p.

Mahan, K.H., Goncalves, P., Williams, M.L. and Jercinovic, M. J., 2006. Dating metamorphic reactions and fluid flow: application to exhumation of high-*P* granulites in a crustal-scale shear zone, western Canadian Shield. J. Metam. Geol., 24, 193-217.

McFarlane, C.R.M., Connelly, J.N., Carlson, W.D., 2006. Contrasting response of monazite and zircon to a high-T thermal overprint. Lithos, 88, 135-149.

Meert, J.G., 2003. A Synopsis of events related to the assembly of East Gondwana. Precambrain Research, 362, 1-40.

Min, K., Mundil, R., Renne, P.R., Ludwig, K.R., 2000. A test for systematic errors in 40Ar/39Ar geochronology through comparison with U–Pb analysis of a 1.1 Ga rhyolite. Geochimica Cosmochimica Acta, 64, 73–98.

Montel, J.-M., Foret, S., Veschambre, M., Nicollet, C., Provost, A., 1996. A fast, reliable, inexpensive in-situ dating technique: Electron microprobe ages on monazite. Chem. Geol., 131, 37-53.

Pandit, M.K. and de Wall, H., 2010. Geochemistry and magnetic fabric studies of Mt. Abu granitoids in the Aravalli-Delhi foreland – implications for Middle Neoproterozoic crustal convergence in NW India. International Journal of Earth Science. (submitted)

Pandit, M.K., Carter, L.M., Ashwal, L.D., Tucker, R.D., Torsvik, T.H., Jamtveit, B., Bhushan, S.K., 2003. Age, petrogenesis and significance of 1 Ga granitoids and related rocks from the Sendra area, Aravalli Craton, NW India. Journal of Asian Earth Sciences, 22, 363-381.

Parrish, R.R., 1990. U-Pb dating of monazite and its application to geological problems. Can. J. Earth Sci., 27, 1431-1450.

Passchier, C.W. and Trow, R.A.J, 2005. Microtectonics. Springer Verlag Berlin, Heidelberg.

Roy, A.B. and Jakhar, S.R., 2002. Geology of Rajasthan (Northwest India) – Precambrian to Recent. Scientific Publishers (India). Jodhpur, 421p.

Roy, A.B. and Sharma, K.K., 1999. Geology of the region around Sirohi town, western Rajasthan – store of Neoproterozoic evolution of the Trans-Aravalli crust. In: Paliwal, B.S. (ed.) Geological evolution of western Rajasthan. Scientific Publishers (India), Jodhpur,19-33.

Schandl, E.S. and Gorton, M.P., 2004. A textural and geochemical guide to the identification of hydrothermal monazite: criteria for selection of samples for dating epigenetic hydrothermal ore deposits. Econ. Geol., 99, 1027–1035.

Schulz, B., 2009. EMP-monazite age controls on P-T paths of garnet metapelites in the Variscan inverted metamorphic sequence of La Sioule, French Massif Central. Bulletin de la Societe Geologique de France, 180, 3, 171-182.

Schulz, B., Braetz, H., Bombach, K. and Krenn, E., 2007. In situ Th-PB dating of monazite by 266 nm laser ablation and ICP-MS with a single collector, and its control by EMP analysis. Zeitschrift fuer Geologische Wissenschaften, 35, 6, 377-392.

Seydoux-Guillaume, A.-M., Paquette, J.-L., Wiedenbeck, M., Montel, J.-M. and Heinrich, W., 2002. Experimental resetting of the U -Th-Pb system in monazite. Chemical Geology, 191, 165-181.

Sharma, K. K., 2004. The Neoproterozoic Malani Magmatism of the northwestern Indian shield: Implications for crust building processes. J Earth Syst Sci, 113, 795 – 807.

Sharma, K.K. 1996.Stratigraphy, structure and tectonic evolution of the metasediments and associated rocks of the Sirohi region, southwestern Rajasthan. Unpublished Ph. D. thesis, Mohanlal Sukhadia University, Udaipur, 103p.

Shelley, D., 1993. Igneous and metamorphic rocks under the microscope. Chapman and Hall, London.

Simpson, C. and Wintsch, R. P., 1989. Evidence for deformation-induced K-feldspar replacement by myrmekite. Journal of Metamorphic Geology, 7, 261-275.

Steiger, R.H., Jäger, E., 1977. Subcommission on geochronology: convention on the use of decay constants in geo- and cosmochronology. Earth and Planetary Science Letters, 36, 359-362.

Suzuki, K. and Kato, T., 2008. CHIME dating of monazite, xenotime, zircon and polycrase: Protocol, pitfalls and chemical criterion of possibly discordant age data. Gondwana Research, 14, 4, 569-586.

Suzuki, K., Adachi, M. and Kajizuka, I., 1994. Electron microprobe observations of Pb diffusion in metamorphosed detrital monazites. Earth and Planetary Science Letters, 128, 391-404.

Tchato, D.T., Schulz, B. and Nzenti, P., 2009. Electron microprobe dating and thermobarometry of Neoproterozoic metamorphic events in the Kekem area, Central African Fold Belt of Cameroon. Neues Jahrbuch Mineralogie, 185/3, 95-109.

Torsvik, T.H., Carter, L.M., Ashwal, L.D., Bhushan, S.K., Pandit, M.K., Jamtveit, B., 2001. Rodinia refined or obscured: Palaeomagnetism of the Malani Igneous Suite (NW India). Precambrian Research, 108, 319-333.

van Lente, B., Ashwal, L.D., Pandit, M.K., Bowring, S.A. and Torsvik, T.H., 2009. Neoproterozoic hydrothermally altered basaltic rocks from Rajasthan, northwest India: Implications for late Precambrian tectonic evolution of the Aravalli Craton. Precambrian Research, 170, 3-4, 202-222.

Williams, M.L., Jercinovic, M.J., Goncalves, P., Mahan, K., 2006. Format and philosophy for collecting, compiling, and reporting microprobe monazite ages. Chem. Geol., 225, 1-15.

Fig. 1: *Geological map of (**a**) Delhi Fold Belt region to Malani Igneous Suite (MIS) transition in NW India with locations of the Erinpura granitoids and (**b**) sampling locations (1: Sirohi Road Section shear zone (SRS); 2: Erinpura migmatite (SI); 3: Syiawa Granite (SY)). ???: unclear tectonic contact between Malani rocks and Erinpura migmatite.*

Fig. 2: ***(a) – (c)**: Progressive mylonitization of coarse-grained Erinpura granite-gneiss (protolith) to mylonite and ultramylonites in the SRS shear zone as seen on the gradual change in structural fabric. Thin section analysis (compare Fig. 3) clearly revealed the ductile nature of the shear process. (**d**): Migmatite SE of Sirohi (compare Fig.1) with leucosome (bright schlieren) and restites (dark parts) indicating the beginning of melting. (**e**): Transition from migmatite to anatectic granite in the Erinpura terrane indicating a mobilization of larger amount of melt.*

Fig. 3:

*Microscopic photographs (crossed nicols) of (**a**) protolith, (**b**) mylonite and (**c**) ultramylonite from the SRS shear zone with a distinct grain size reduction due to a progressive mylonitization. (**a**) Microfractures in K-feldspar grains are filled with recrystallized phases such as feldspar, quartz and muscovite indicating deformation under brittle to ductile conditions. Anatectic granite formed during migmatization of the Erinpura-type granite (**d.** and **e.**) and the Siyawa Granite (**f**) reveal structures (myrmekite formation, dynamic*

*recrystallization, weak foliation) that indicate a syn-intrusional deformation under medium-grade conditions: (**d**) Feldspar σ-clast and weakly developed foliation, (**e**) deformation bands and myrmekite formation that is favoured within small shear zones indicating strain, (**f**), Feldspar in the Siyawa Granite with core and mantle structures, quartz inclusion with strain induced perthitic exsolution indicating deformation during crystallization.*

Fig. 4: *Backscattered electron (BSE) image of (**a**) large magmatic monazite in the Erinpura protolith (SR-1) from the SRS shear zone. The monazite shows compositional heterogeneities with Th-rich (light) zones and internal cracks, which triggered a (hydro-) thermal overprint. (**b**) Aggregate of small new monazite grains in the same sample (SR-1) which crystallized with irregular shapes in biotite-rich domains. (**c**) Deformed aggregate in a mylonite sample (JB) of apatite, epidote and Th-rich silicate formed due to the decomposition of monazite during mylonitization. (**d**) Monazite grain that occurs within feldspar in anatectic granite. (**e**) Altered monazite grain that is associated with biotite and coronas of apatite, Th-silicates and epidote in anatectic granite. (**f**) One of the two old monazite grains found in the Siyawa Granite. (**g**) Overprinted grain in the Siyawa Granite: bright areas are older (~811 Ma) and show low Si but high Th contents. Grey areas are younger (~768 Ma or younger) with low Si and Th contents (compare also Fig. 6b).*

Fig. 5: *Th-U-Pb CHIME model ages of different monazite grain populations shown as total PbO vs. ThO_2* isochrone diagrams and histograms of (**a**) Erinpura protolith (SR-1) and mylonite (JB) from the SRS shear zone, (**b**)*

*anatectic granite and (**c**) Siyawa Granite. *ThO_2 is ThO_2 plus UO_2 equivalents expressed as ThO_2, after Suzuki et al. (1994). Slopes of linear retrogressions of the compositional data represent isochrone ages which correspond to weighted mean ages from single data points. Note accumulation of ages at 770-780 Ma and 740 Ma as accented in histograms.*

Fig. 6: *Mineral chemistry of monazite generations vs. Th-U-Pb chemical ages of Erinpura type granitoids from (**a**) Sirohi area and (**b**) Siyawa Granite in the Delhi Fold Belt. Please see text for further explanation.*

Fig. 7: *$^{40}Ar/^{39}Ar$ muscovite age spectra of a mylonite (RT-01) from the SRS shear zone near Sirohi town. Results are replotted and recaclculated. Note the plateau indicating a 736 ± 6 Ma (MSWD = 0.62, P = 0.76) old cooling of the shearing.*

Fig. 8: *Timetable for the tectono-thermal history in the Erinpura terrane. Please see text for further explanation.*

Fig. 9: *A model of a probable scenario during the formation of the SRS shear zone and the migmatites. The stereoplots are projections in the lower hemisphere. Great circles represent foliations and dark squares represent mineral lineations.*

Table

Table 1: Electron microprobe analyses of monazite

Sample	SiO_2	P_2O_5	CaO	Y_2O_3	La_2O_3	Ce_2O_3	Pr_2O_3	Nd_2O_3	Er_2O_3	ThO_2	UO_2	PbO	Total	Th
Siyawa Granite														
sy4-3sm3	0.95	30.59	2.74	2.35	13.51	23.91	2.16	8.10	0.12	13.00	0.99	0.54	101	11.42
sy4-7-1	0.83	29.46	2.65	2.03	13.73	24.01	2.30	7.92	0.07	13.55	0.95	0.56	100	11.91
sy4-7-6	0.42	30.24	2.86	2.34	13.41	23.79	2.30	7.91	0.09	12.65	1.29	0.53	100	11.12
sy4-8-1	1.69	28.48	2.45	0.74	12.69	25.29	2.44	9.00	0.07	13.82	0.72	0.58	101	12.15
sy4-24-3	1.03	28.70	3.51	1.68	13.59	23.67	2.17	7.86	0.13	13.16	1.52	0.59	100	11.57
Anatectic derivative of Erinpura Granite														
si3c-6-1	2.67	26.84	0.94	0.50	15.38	27.19	2.53	9.04	0.13	14.55	0.21	0.51	102	12.79
si3c-6-3	1.04	29.54	1.93	1.73	13.80	25.61	2.48	8.96	0.16	11.59	0.54	0.45	100	10.19
si3c-8-1	1.41	28.50	1.81	1.50	14.38	26.22	2.49	9.00	0.18	11.50	0.41	0.43	100	10.11
si3c-11-1	1.81	27.43	0.81	1.77	15.09	27.51	2.66	9.37	0.17	9.89	0.14	0.34	100	8.69
si3c-11-2	1.82	27.61	0.91	1.99	14.75	27.11	2.62	9.29	0.18	10.27	0.22	0.35	100	9.03
Mylonites from shear zone (SRS) in Erinpura Granite														
JB-1-2	0.37	29.53	0.66	1.52	15.34	29.72	2.97	11.49	0.18	3.20	0.16	0.13	99	2.82
JB-8-1	0.37	30.52	0.74	2.08	14.52	29.32	3.04	11.72	0.23	2.52	0.36	0.13	100	2.21
SR1-2-1-2	0.31	29.71	0.44	2.41	14.36	29.28	3.08	12.22	0.18	2.50	0.18	0.10	99	2.20
SR1-2-5-4	0.45	29.22	0.61	1.99	13.56	28.91	3.05	12.54	0.21	3.43	0.22	0.14	98	3.01
SR1-2-5-6	0.26	29.16	0.84	2.43	13.22	28.36	3.04	12.46	0.21	2.95	0.46	0.15	98	2.59
SR1-1-93	0.86	28.63	2.09	0.22	12.38	26.59	2.83	10.61	0.11	11.52	0.31	0.46	100	10.13
SR1-1-94	0.88	28.66	2.14	0.22	12.34	26.33	2.81	10.60	0.13	11.99	0.30	0.45	100	10.54
SR1-1-95	0.79	28.96	1.86	0.37	12.76	27.19	2.92	10.88	0.14	10.55	0.24	0.42	100	9.27
SR1-1-96	0.65	29.12	2.07	0.21	12.73	26.77	2.87	10.56	0.13	10.79	0.28	0.40	100	9.49
SR1-1-99	0.53	28.92	1.32	2.00	13.15	27.22	2.86	11.76	0.19	6.98	0.12	0.25	98	6.13
SR1-1-100	0.56	29.61	1.45	2.48	12.53	25.94	2.85	11.44	0.15	8.07	0.14	0.29	99	7.09
SR1-1-102	0.78	28.83	1.90	0.37	12.76	26.88	2.94	10.97	0.14	10.55	0.23	0.37	100	9.27
SR1-1-109	0.64	29.30	1.65	0.98	13.26	27.39	2.82	10.93	0.14	8.95	0.17	0.35	100	7.86
SR1-2-111	0.67	29.18	1.44	2.57	12.73	26.23	2.74	10.87	0.12	8.32	0.16	0.33	99	7.31
SR1-6-128	0.75	28.97	1.59	1.03	12.97	26.94	2.93	11.19	0.12	9.18	0.18	0.37	99	8.07

Th* is calculated from Th and U after Suzuki et al. (1994).

Figure
Click here to download high resolution image

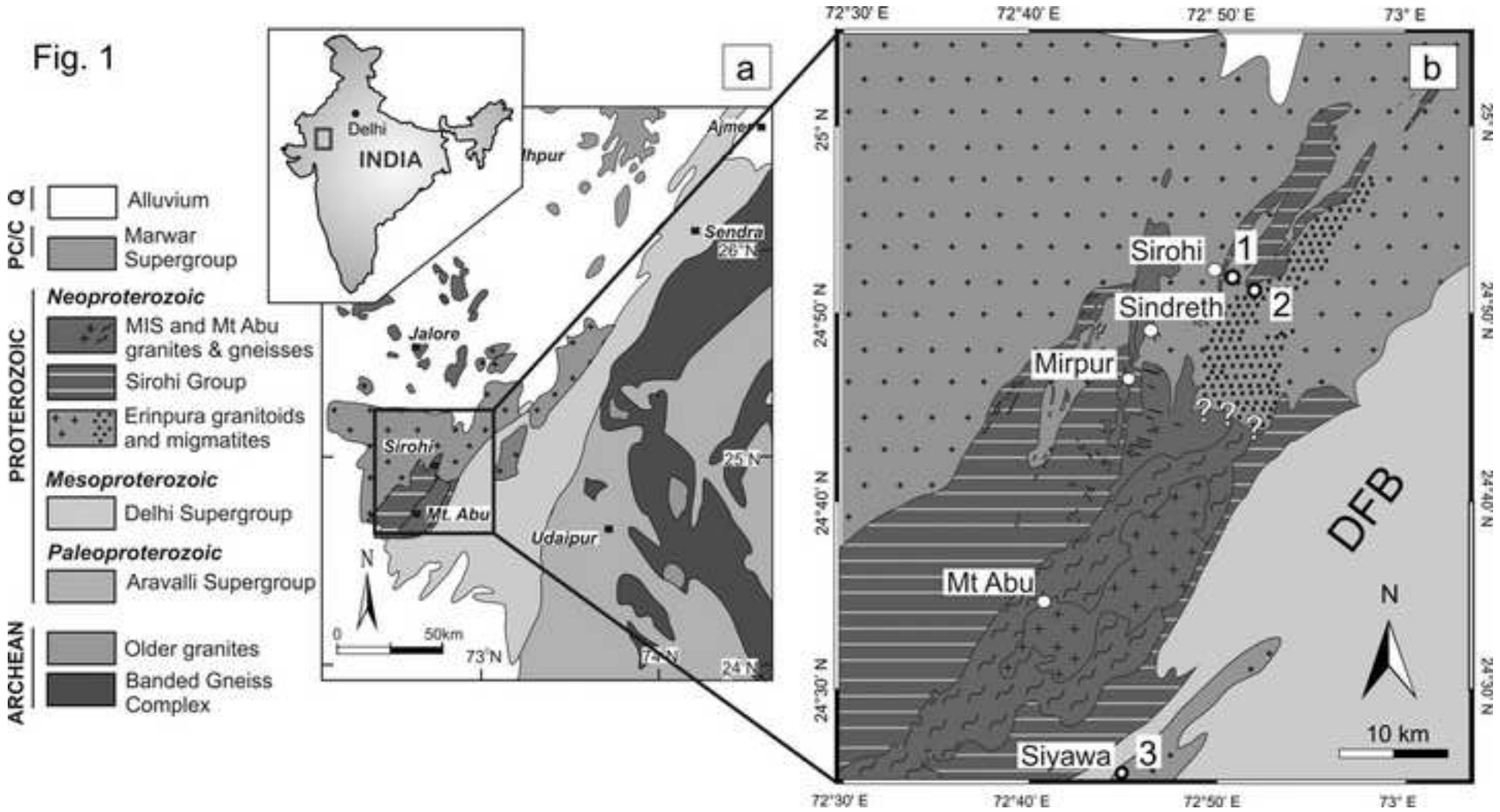

Figure
Click here to download high resolution image

Fig. 2

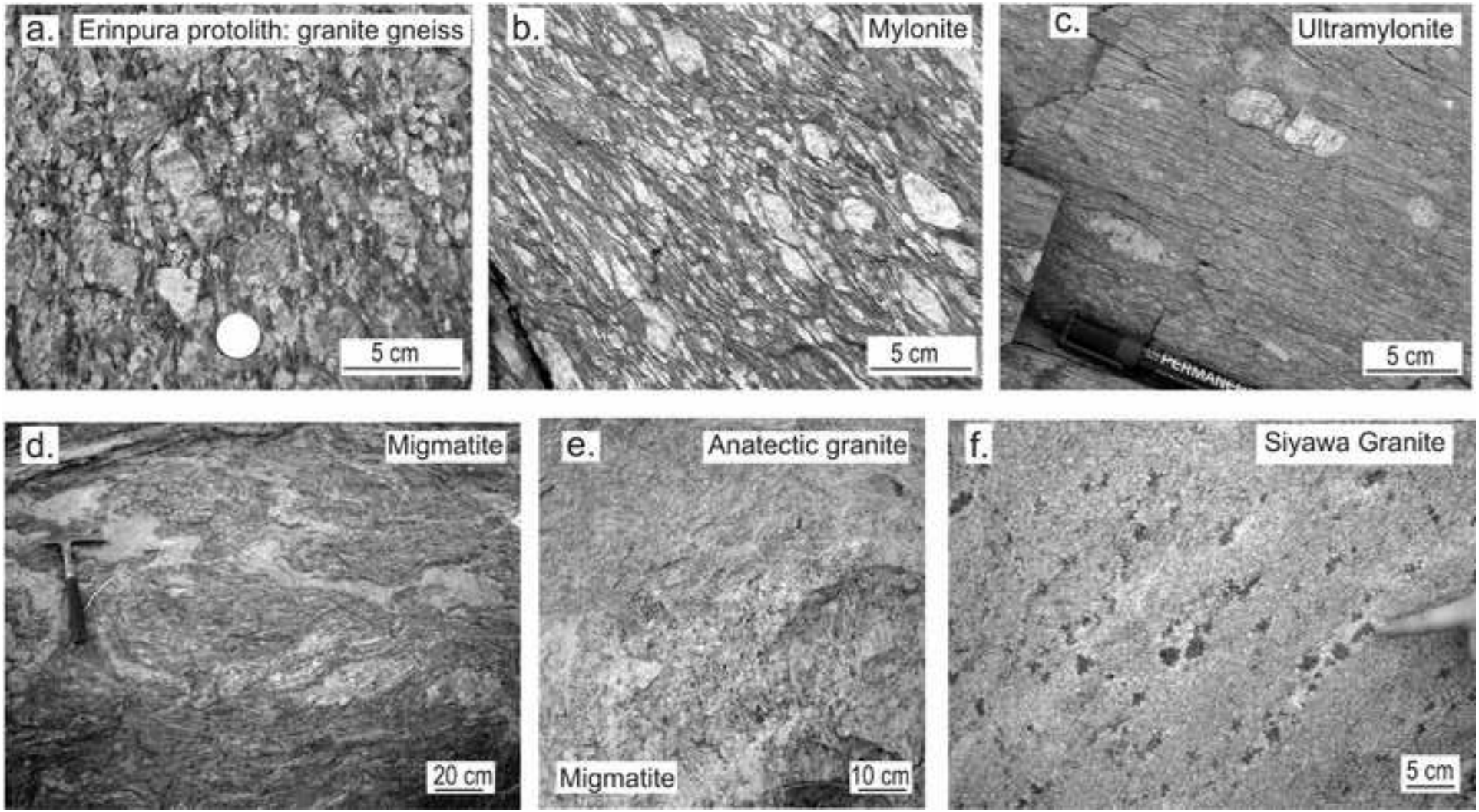

Figure
Click here to download high resolution image

Fig. 3

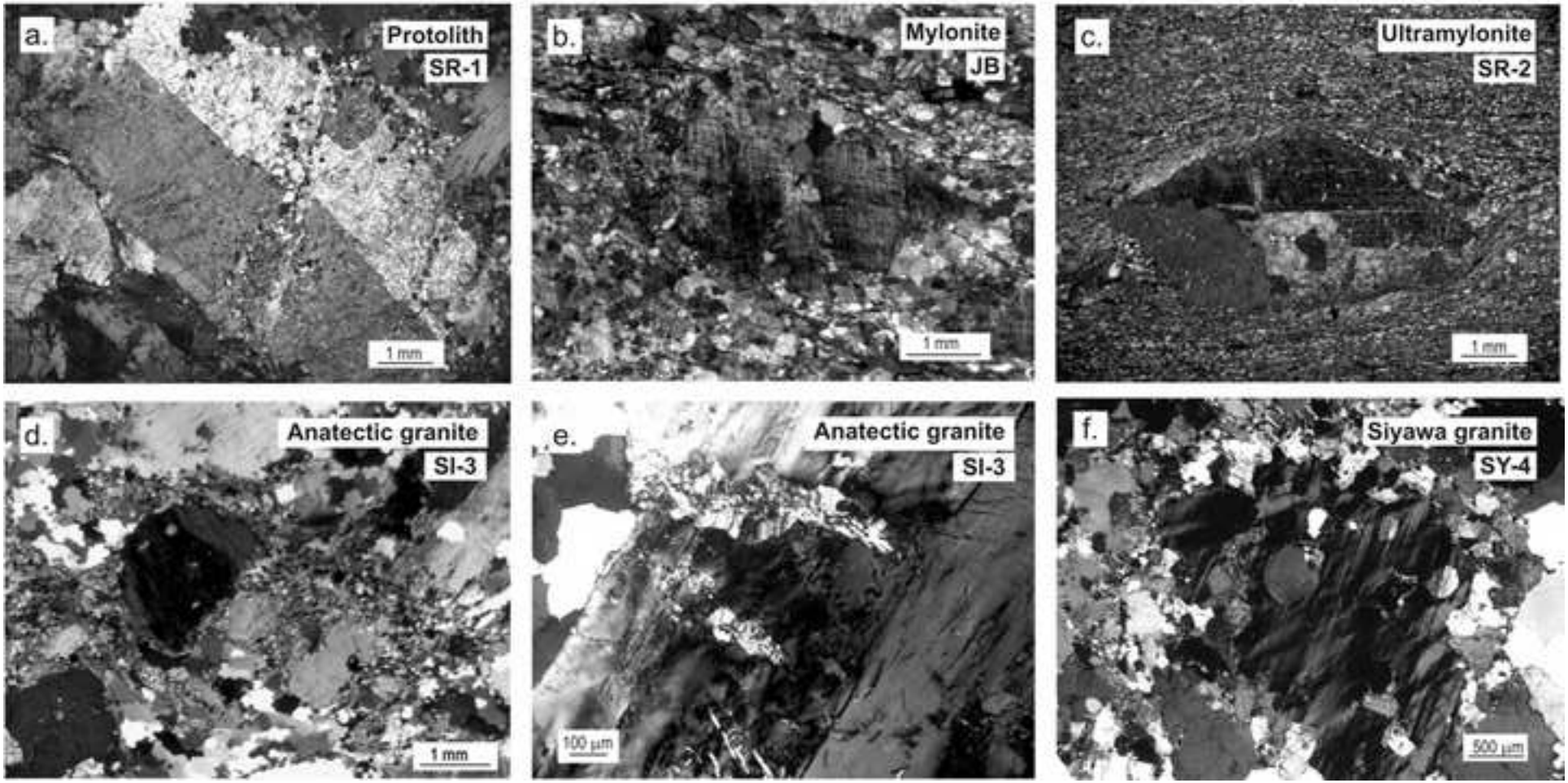

Figure
Click here to download high resolution image

Fig. 4

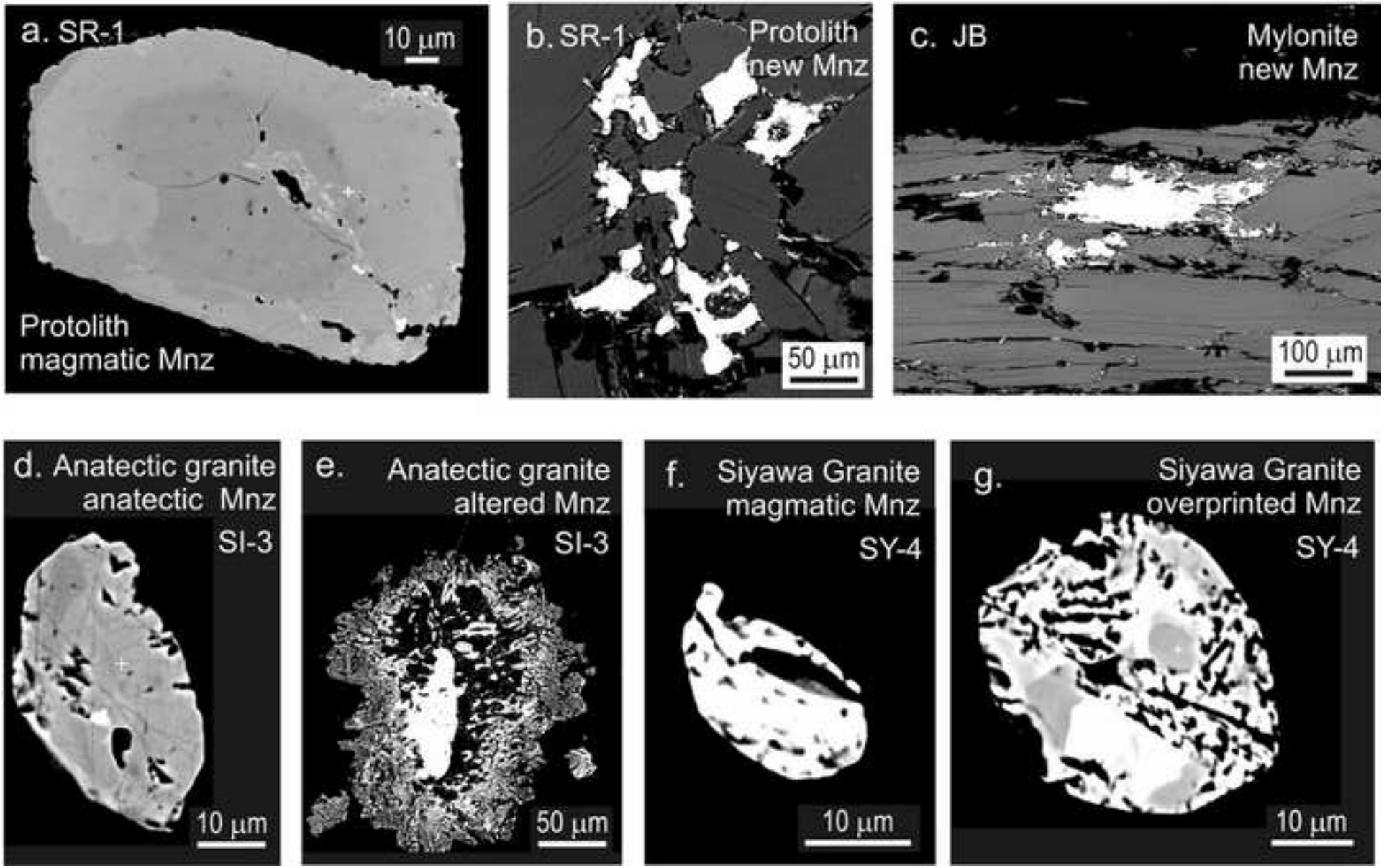

Figure

Click here to download high resolution image

Fig. 5

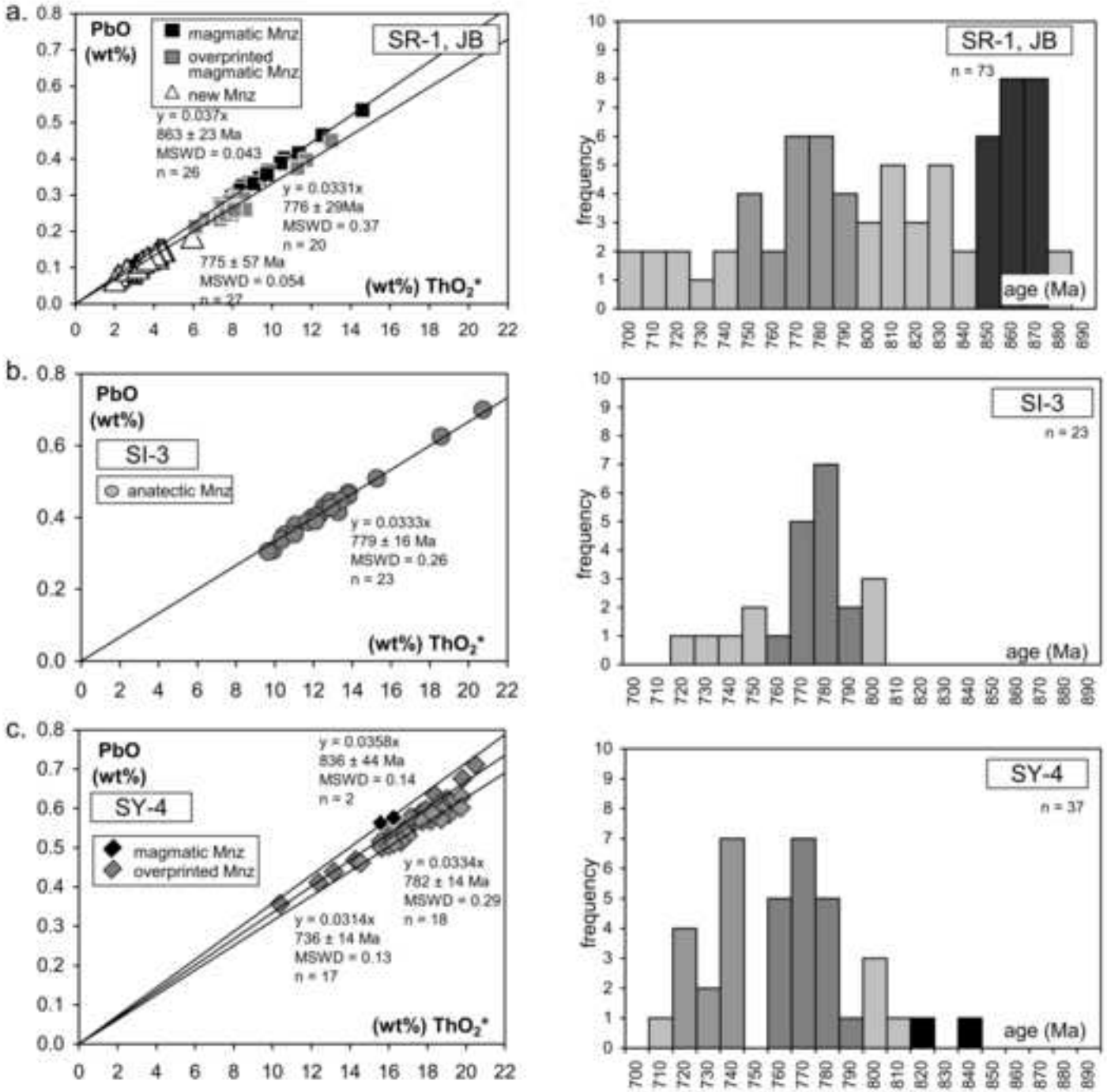

Figure

Click here to download high resolution image

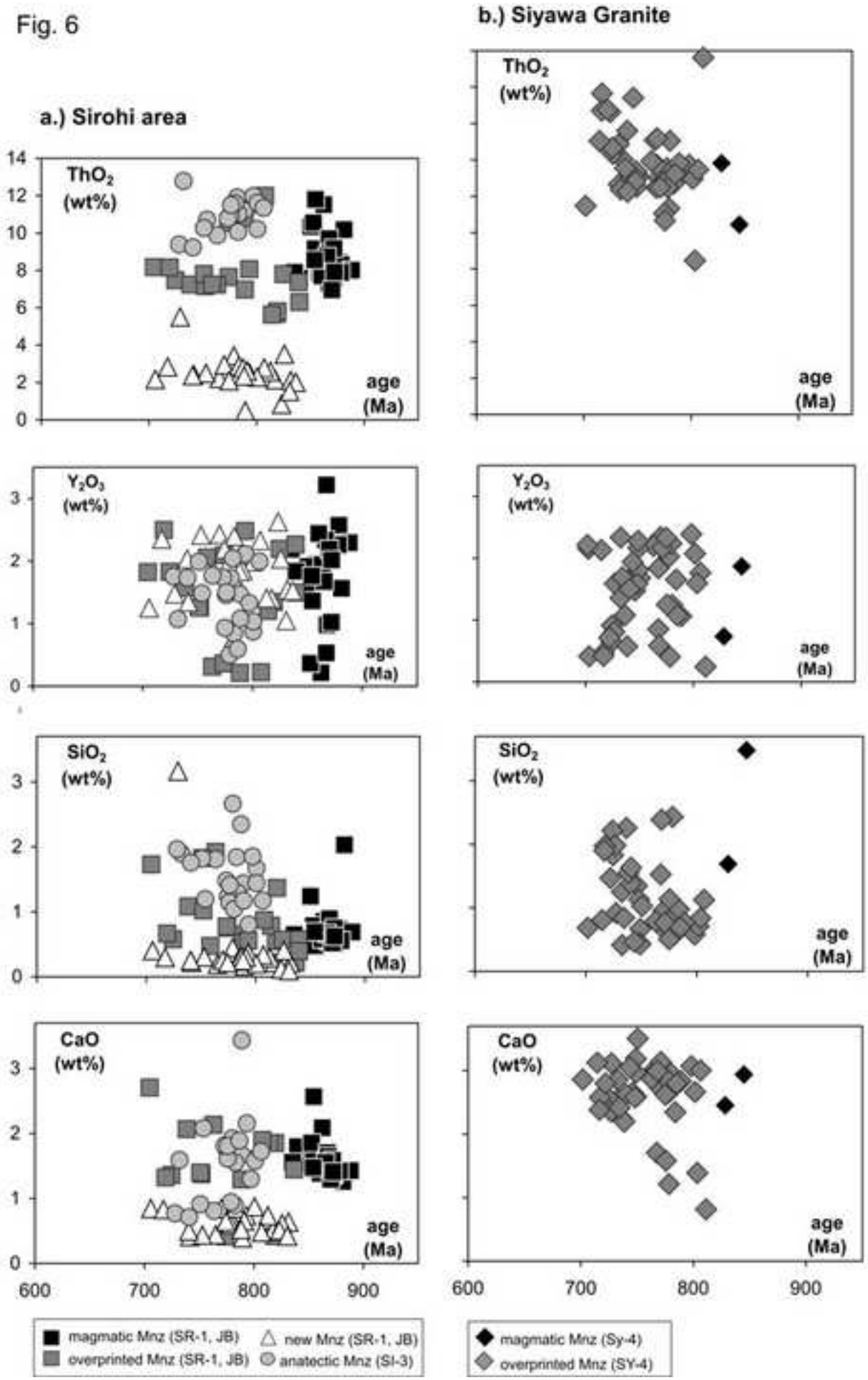

Figure

Click here to download high resolution image

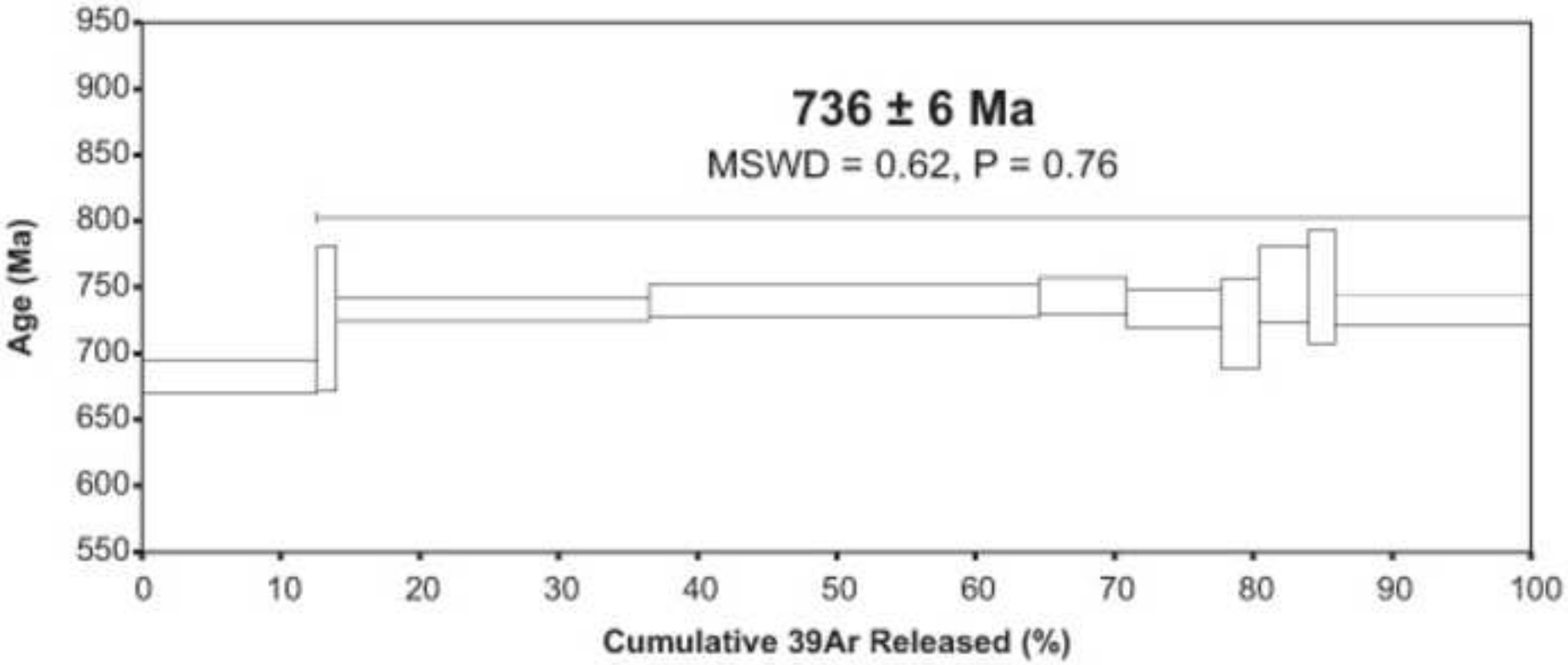

Figure
Click here to download high resolution image

Fig. 8

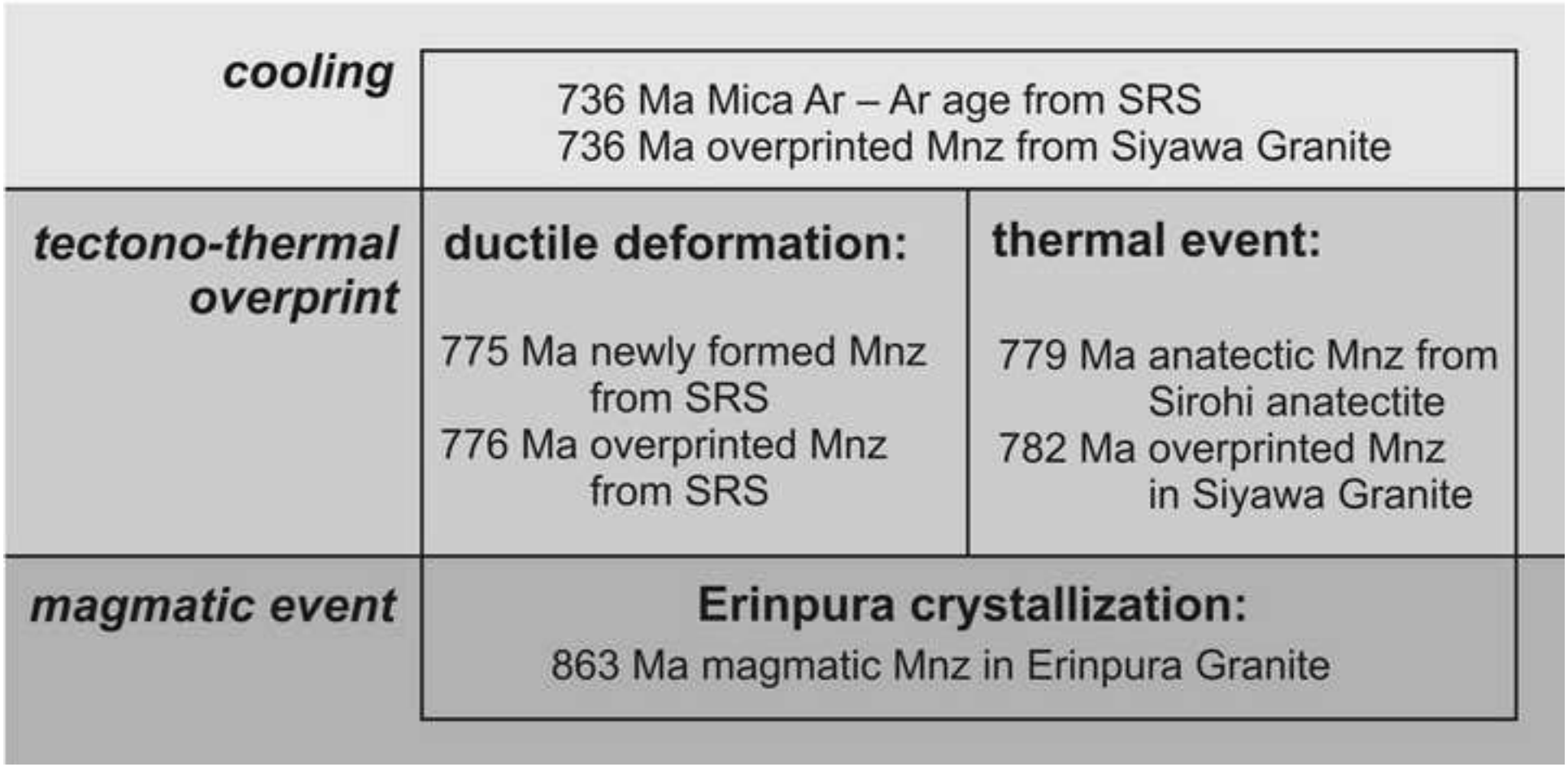

Figure
Click here to download high resolution image